Received: 3 June 2021 | Revised: 27 July 2021 | Accepted: 8 August 2021

DOI: 10.1002/inf2.12250

ORIGINAL ARTICLE

WILEY

Mechanoluminescent hybrids from a natural resource for energy-related applications

Chunfeng Wang[1,2] | Ronghua Ma[1] | Dengfeng Peng[1] | Xianhu Liu[3] | Jing Li[2] | Boru Jin[2] | Aixian Shan[4] | Yu Fu[1] | Lin Dong[3] | Wenchao Gao[5] | Zhong Lin Wang[2] | Caofeng Pan[1,2]

[1]Key Laboratory of Optoelectronic Devices and Systems of Ministry of Education and Guangdong Province, College of Physics and Optoelectronic Engineering, Shenzhen University, Shenzhen, China

[2]CAS Center for Excellence in Nanoscience, Beijing Key Laboratory of Micro-nano Energy and Sensor, Beijing Institute of Nanoenergy and Nanosystems, Chinese Academy of Sciences, Beijing, China

[3]Key Laboratory of Materials Processing and Mold (Ministry of Education), Henan Key Laboratory of Diamond Optoelectronic Materials and Devices, Key Laboratory of Material Physics, Ministry of Education, School of Physics and Microelectronics, Zhengzhou University, Zhengzhou, China

[4]Beijing Advanced Innovation Center for Materials Genome Engineering, Beijing Key Laboratory for Magneto-Photoelectrical Composite and Interface Science, School of Mathematics and Physics, University of Science and Technology Beijing, Beijing, China

[5]Department of Civil Engineering, Monash University, Clayton, Australia

Correspondence
Dengfeng Peng, Key Laboratory of Optoelectronic Devices and Systems of Ministry of Education and Guangdong Province, College of Physics and Optoelectronic Engineering, Shenzhen University, Shenzhen 518060, China.
Email: pengdengfeng@szu.edu.cn

Wenchao Gao, Department of Civil Engineering, Monash University, Clayton 3800, Australia.
Email: wenchao.gao1@monash.edu

Zhong Lin Wang and Caofeng Pan, CAS Center for Excellence in Nanoscience, Beijing Key Laboratory of Micro-nano Energy and Sensor, Beijing Institute of Nanoenergy and Nanosystems, Chinese Academy of Sciences, Beijing 100083, China.
Email: zlwang@binn.cas.cn; cfpan@binn.cas.cn

Abstract

Mechanoluminescent (ML) materials that directly convert mechanical energy into photon emission have emerged as promising candidates for various applications. Despite the recent advances in the development of both novel and conventional ML materials, the limited access to ML materials that simultaneously have the attributes of high brightness, low cost, self-recovery, and stability, and the lack of appropriate designs for constructing ML devices represent significant challenges that remain to be addressed to boost the practical application of ML materials. Herein, ML hybrids derived from a natural source, waste eggshell, with the aforementioned attributes are demonstrated. The introduction of the eggshell not only enables the preparation of the hybrid in a simple and cost-effective manner but also contributes to the homochromatism (red, green, or blue emission), high brightness, and robustness of the resultant ML hybrids. The significant properties of the ML hybrids, together with the proposed structural design, such as porosity or core–shell structure, could expedite a series of mechanic-optical applications, including the self-luminous shoes for the conversion of human motions into light and light generators that efficiently harvest water wave energy. The fascinating properties, versatile designs, and the efficient protocol of "turning waste into treasure" of the ML hybrids represent significant

Chunfeng Wang and Ronghua Ma contributed equally to this work.

Funding information
Science and Technology Innovation Project of Shenzhen Excellent Talents, Grant/Award Number: RCBS20200714114919006; Shenzhen Fundamental Research Project, Grant/Award Numbers: 201708183000260, JCYJ20190808170601664; Natural Science Foundation of Beijing Municipality, Grant/Award Number: Z180011; Fundamental Research Project of Guangdong Province, Grant/Award Number: 2020A1515011315; National Natural Science Foundation of China, Grant/Award Numbers: 52125205, 52002246, 61505010, 61804011, 61805015, 51432005, 51622205, 61675027, U20A20166, 61875136

advances in ML materials, promising a leap to the practical applications of this flouring material family.

KEYWORDS
blue energy harvesting, eggshell waste, mechanoluminescent hybrids, smart sensing

1 | INTRODUCTION

Stimuli-responsive materials (SRMs), whose characteristics can be switched using an external stimulus such as electricity, light, heat, and mechanical energy, underpin emerging technologies ranging from sensors, actuators, generators, to energy harvesters.[1,2] In particular, as a class of SRMs with a long history, inorganic mechanoluminescent (ML) materials that can repeatedly convert mechanical energy into photon emission with excellent performances have been re-emerging for their potential applications in sensing,[3–6] displays,[7–12] and as special light sources.[13,14] During the last decade, many endeavors have been dedicated to the development of new ML materials with different lanthanide ions paired with different substrates for realizing versatile ML emissions.[15] For example, the Pr^{3+}-doped $LiNbO_3$ exhibits red ML emission without a strain threshold[16]; the Pr^{3+}- and Er^{3+}-doped $NaNbO_3$ exhibits the multimode emissions[17,18]; and the Nd^{3+}-doped $Sr_3Sn_2O_7$ shows a near-infrared ML emission.[19–21] Meanwhile, significant progress has been made in the renewed utilization of certain conventional ML materials such as transition-metal-doped ZnS. For example, Pan et al. developed an electronic signature device based on ZnS ML materials annealed in vacuum[3]; Jeong et al. demonstrated the wind-driven displays by incorporating ZnS into PDMS pillars[22]; Hao et al. obtained the active ML emissions by coupling ZnS powder with either an electronic field or a magnetic field[23,24]; Song et al. reported a skin-driven ML stickers using SiO_2-enhanced ZnS materials[25]; Hong et al. demonstrated the ultrasonically driven ML emission of nanosized ZnS for minimally invasive optogenetic neuromodulation.[26,27] In addition, our group has previously demonstrated tunable ML emission across the full visual spectrum using CaZnOS, which has Ca sites that are suitable for the doping of almost all lanthanide ions (>10 types).[28,29] Despite these achievements, the practical implementation of ML materials still encounters many challenges and lags behind the discovery of materials themselves. This can be ascribed to the limited access to ML materials that simultaneously have the attributes of high brightness, low cost, self-recovery, and stability, as well as the lack of appropriate architectural designs the targeted applications.

Herein, we demonstrate high-performance ML hybrids with the corresponding structural designs for energy-related applications such as the mechanical energy-to-light conversion of human motions and blue energy harvesting. Innovatively, in this study, we utilized eggshell wastes as the raw material for the simple and mass production of ML hybrids composed of ZnS and CaZnOS with a series of advantages: (i) the three primary color emissions, namely, red (R), green (G), and blue (B), originating from the abundantly available activators incorporated into the cation sites of both ZnS and CaZnOS in the hybrid, in which the reproducible deep blue ML with the peak wavelength of 420 nm is realized from this system for the first time. (ii) A self-recoverable and intense ML emission because of the efficient charge transfer and recombination owing to the energy band offset at the interface of the hybrid. (iii) High stability against water and ethanol owing to the intrinsic resistance of the oxysulfides to water and ethanol, as well as the interface lattice strain between ZnS and CaZnOS. (iv) A simple and efficient synthetic method that does not require high vacuum or reduced atmosphere profiting from the oxygen-embedded nature of the oxysulfides. Most importantly, using this ML hybrid, a self-powered sen-memory panel and a self-luminous sponge with the porous structure were designed for the mechanical energy-to-light conversion using human motions. Further, an in situ growth strategy of ML hybrid@ZrO_2

core–shell beads was developed for the assembly of a light generator for the efficient harvesting of water wave energy. This work provides a concise approach to the realization of high-performance ML materials with a designed architecture, promising their practical applications in smart displays and wearable devices via mechanical energy utilization, and simultaneously turning waste into treasure.

2 | RESULTS AND DISCUSSION

2.1 | Eggshell-assisted synthesis of ML hybrids

The global food processing industry consumes an estimated one billion eggs per day,[30] and a large volume of eggshells is discarded as wastes due to the lack of an

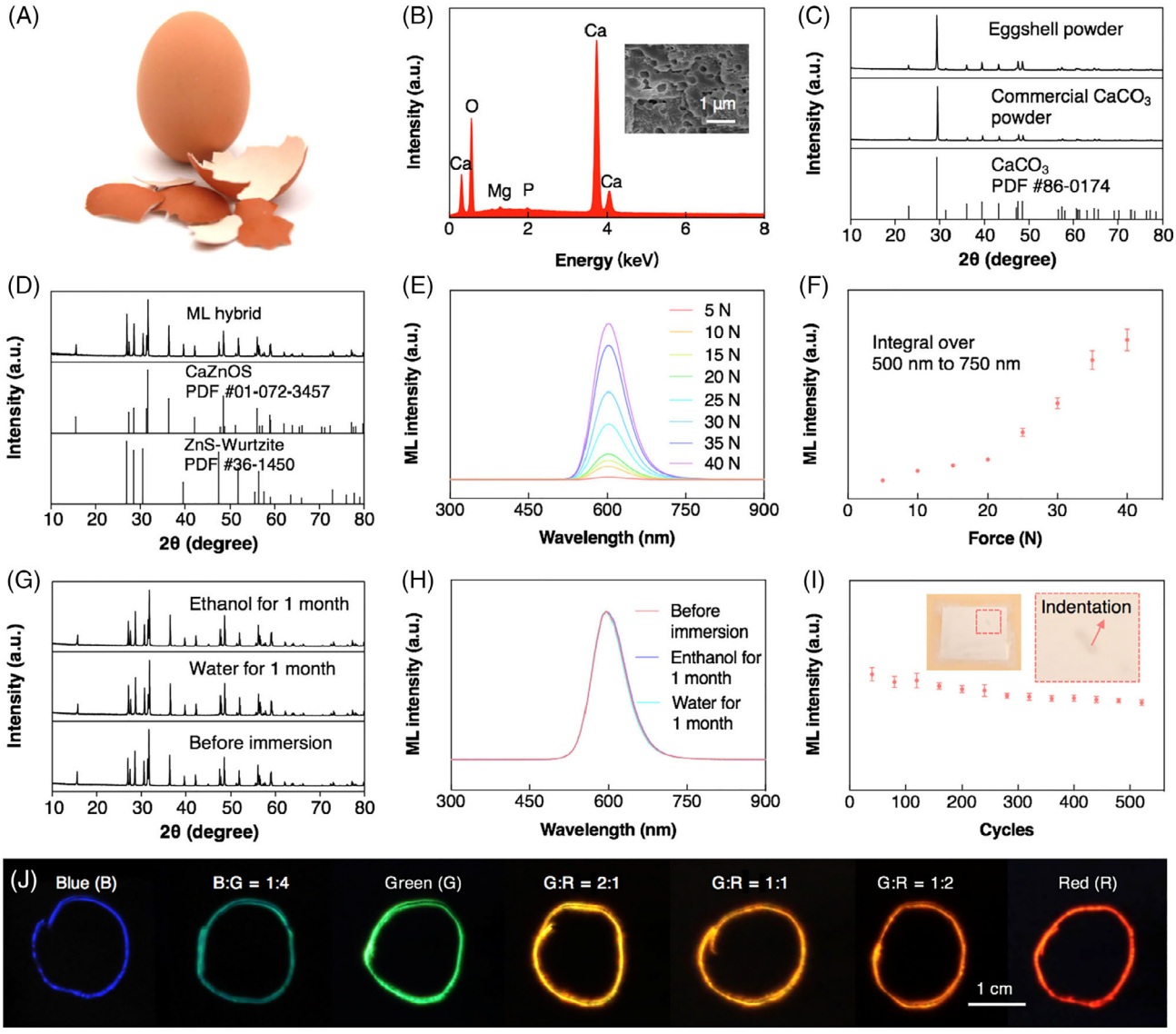

FIGURE 1 Eggshell-assisted synthesis of the ML hybrids. (A) A photograph of the eggshells used for the synthesis of the ML hybrids. (B) The EDS spectrum of the eggshells showing the preponderant composition of calcium carbonate. Inset shows the SEM image of the eggshell with the distributed circular pores. (C) The XRD patterns of the as-synthesized eggshell powder and the commercial calcium carbonate powder, showing the unanimous diffraction peaks that are well indexed to the standard one. (D) The XRD patterns of the optimized ML hybrids, whose diffraction peaks are well indexed to the standard ones of either CaZnOS or ZnS. (E) The ML spectra of the optimized ML hybrids as a function of the applied forces. (F) The integral emission intensity from 500 to 750 nm and the corresponding emission images of the optimized ML hybrids under different forces. (G,H) The XRD patterns and ML spectra of the optimized ML hybrids before and after immersing in water and ethanol for 1 month, which do not show obvious difference. (I) The ML intensity of the optimized ML hybrids as stress of 40 N is applied repeatedly. (J) The color regulation achieved by mixing the three-primary color ML hybrids of Mn-, Pr-, and Pb-doped ZnS-CaZnOS with the different weight ratio

efficient approach to utilize them. Eggshells are generally disposed of in landfills, leading to odor production and microbial growth; they thus pose the risk of environmental pollution and pathogen propagation. Therefore, the development of a suitable approach for converting eggshells into valuable materials is indispensable for achieving environmental and economic benefits. In this study, eggshells with a porous structure and preponderant composition of calcium carbonate (Figure 1A,B) were collected from the local market and processed into the eggshell powder (see Section 4 for details). The eggshell powder exhibited an x-ray diffraction (XRD) pattern that agreed well with that of the commercial calcium carbonate powder (Figure 1C). The eggshell powder was utilized in conjunction with the ZnS powder and the corresponding dopant (Mn is selected here as an example) for the high-temperature solid-state synthesis of ML hybrids (see Section 4). Specifically, the weight ratio of eggshell to ZnS powder was varied to obtain biphasic CaZnOS–ZnS hybrids, as determined by XRD analyses (Figure 1D); the diffraction peaks of the hybrids could be indexed well to the standard peaks of CaZnOS (PDF #01-072-3547) and ZnS (PDF #36-1450). The particle size of the ML hybrids was found to be distributed in the range of 1–6 μm (Figure S1). The segregation of calcium and zinc, as indicated by the energy-dispersive x-ray spectroscopy (EDS) mapping image (Figure S2), and the origination of two distinct emission colors from a single ML particle, as observed in the fluorescence microscope images (Figure S3), further confirmed the biphasic nature of the ML hybrids. The x-ray photoelectron spectroscopy (XPS) spectra of the ML hybrids suggested the incorporation of Mn into the hybrids with the bonding states of Mn 2p (Figure S4). The transient photoluminescence decay curves of the ML hybrids revealed that the Mn was distributed in both the CaZnOS and ZnS phases, as determined by the different delay lifetimes of 615 nm and 580 nm emissions, respectively (Figure S5).

The light-emitting performance of the ML hybrids is highly dependent on the molar ratio of the $CaCO_3$ to ZnS in the raw materials, as well as the doping concentration of Mn, as presented in Figure S6. The $CaCO_3$ content in the eggshell powder was estimated to be 90 wt%, and the doping concentration of Mn ranged from 0.2 to 5 mol% with respect to $CaCO_3$. The ML hybrid with a $CaCO_3$:ZnS ratio of 1:2 and a doping concentration of 1 mol% displayed the optimal ML emission intensity, ascribing to the enlarged area of the heterogeneous interface between CaZnOS and ZnS and the immune concentration quenching effect in the hybrid.[29] The emission intensity of the optimized ML hybrid was two times higher than the commercial Mn-doped ZnS ML material (Figure S7), and remarkably, the optimized hybrid exhibited a bright emission with a vivid color under multiple mechanical stimuli such as shaking, pricking, and grinding (Videos S1–S3). The ML spectra of the optimized ML hybrids as a function of the applied forces are depicted in Figure 1E, according to which the hybrids could be illuminated at a low force of 5 N, and the ML emission intensity increased with increasing force. The response of ML to the applied force was nonlinear, with two different slopes at different force regions (Figure 1F), which can be attributed to the combined ML mechanisms of triboluminescence and piezoluminescence.

In fact, the ML mechanism remains elusive, and has been phenomenologically or semiempirically attributed to the piezo-phototronic effect, triboelectric effect, or dislocation motion.[3,31–35] The operational mechanism of ML materials with piezoelectric hosts such as ZnS and CaZnOS has been predominantly assigned to piezoelectricity-induced carrier de-trapping. However, the piezoelectric field generated within these materials by the threshold pressure was found to be of the order of 10^3 V cm^{-1} and may not cause ML emission (Appendix S1).[36] A model based on a local piezoelectric field near the dopant ions has been proposed, with a piezoelectric filed of the order of 10^4 V cm^{-1} due to the higher piezoelectric constant caused by the higher structural dissymmetry near the dopant ions,[37] enabling sufficient band bending and sequential ML emission. In this study, we propose that the triboelectric potential generated by the friction between the ML materials and the encapsulation layers or between the ML particles may also contribute to the ML emission, considering the fact that the relative displacement occurred between the ML materials and the encapsulation layers during the measurement of the ML intensity. In fact, Xu et al. have studied the triboluminescence by rubbing the ML materials with the different frictional rods, during which both the triboelectric voltage and the ML intensity depended on the materials of the frictional rods.[31] They proposed that the triboluminescence originated from the electroluminescence induced by the triboelectric field. However, in our case, there is no experimental evidence to support the occurrence of electroluminescence under a triboelectric field, nor to the related report of electroluminescence of the oxysulfides.[38] Thus, the triboluminescence of the oxysulfides can be attributed to the carrier de-trapping caused by the triboelectric potential, and a model can be formulated by simply replacing the piezoelectricity with the triboelectricity in the piezoelectricity-induced carrier de-trapping model. Moreover, the triboelectric voltage of two objects generally shows a nonlinear response to the applied force[39,40] differing from the linear response of the piezoelectric voltage to the force (Figure S8), accounting for the nonlinear relationship between the ML intensity of our

ML hybrids and the applied force. The proposed model is also supported by the enhanced ML emission of a sponge-like sample composed of the hybrid in comparison with that of a nonporous sample, as described in the following section.

The chemical resistance of the ML materials to solvents is highly desired for their application in translation medicine and biology. The ML hybrids remained stable when immersed in water and ethanol, with no apparent deterioration of their crystal structure and ML performance after immersion for 1 month, as indicated by the XRD patterns and ML spectra (Figure 1G,H). The excellent stability benefits from the intrinsic resistance of oxysulfides to water and ethanol,[41,42] as well as the interface lattice strain between ZnS and CaZnOS,[43] enriching the application scopes of ML materials in various fields, such as the photocatalytic water splitting and in vivo bioimaging. The ML hybrids also exhibited excellent mechanical stability, featuring a slight attenuation of ML intensity over 500 cycles of deformation (Figure 1I). The attenuation probably originated from the loose contact of ML particles with the force-applicator rather than from the materials themselves, because repeated application of stress led to the appearance of an indentation, as displayed in the insets of Figure 1I. The biphasic nature of the ML hybrids enriches the availability of activators cooperated into the host, ranging from transitional metal ions to lanthanide ions.[28] In this study, Mn, Pr, and Pb are selected to obtain emissions of the three primary colors emission, namely, red (R), green (G), and blue (B), and the corresponding characterization data of the Pr- or Pb-doped ML hybrids, including the XRD patterns, PL excitation and emission spectra, and ML spectra, are provided in Figures S9, S10, and Video S4. The blue-emitting ML hybrid exhibited an emission with the peak wavelength of 420 nm at an optimized Pb doping concentration of 1 mol%. The versatile color regulation could also be achieved by mixing the three ML materials emitting each of the three primary colors, as presented in Figure 1J.

2.2 | Self-powered, visual sen-memory of the pressure

The favorable attributes of the ML hybrids render them promising for application in self-powered visual sensing of the applied pressure, warranting the identification of the intensity, distribution, and speed of the applied pressure, with clear advantages such as nonintrusiveness, high spatial resolution, in vivo detection, and wireless readout, compared with their counterparts enabled by the electrical principles (Figure S11 and Video S5).[44–48] Despite the aforementioned advances, the sensor device universally besets by the fleeting response to stimuli, thereby requiring continuous physical presentation such as a camera throughout the pressure course, thus imposing a strict limit on the practical applications. Recently, novel ML materials with the memory capabilities enabled by reshuffling the trap occupations of the charge carriers have been demonstrated, endowing the readout of the force-induced light emission, as required.[49,50] However, the readout process is activated either by an infrared laser or by high temperature, impairing their advancement. A simple strategy is proposed here for achieving the self-powdered visual sen-memory of the applied pressure by the combination of the ML hybrid and the long-lasting phosphor of $SrAl_2O_4:Eu^{2+}$, Dy^{3+}, as illustrated in Figure 2A. The light emitted from the ML hybrid in response to the applied force can excite the phosphorescence emission of $SrAl_2O_4:Eu^{2+}$, Dy^{3+}, enabling the record of the applied force over a duration of 1.5 min after the removal of the force (Figures 2B–D and S12). The related sen-memory mechanism is illustrated in Figure 2E, wherein the photoionized electrons travel in the conduction band (CB) and then are captured and stored in the trap levels. The trapped electrons can be released again to CB upon ML radiation and then supplied for the $4f^65d^1$ to $4f^7(^8S_{7/2})$ transition of Eu^{2+} for realizing phosphorescence emission. Note that the applied force can also cause the excitation of the trapped electrons in the shallow trap levels to contribute slightly to the phosphorescence of Eu^{2+}, as indicated by Video S6, in which the control sample is only composed of $SrAl_2O_4:Eu^{2+}$, Dy^{3+} and gives the inconspicuous phosphorescence emission for a short time of a few seconds.

2.3 | Self-luminous sponge for mechanical energy-to-light conversion of human motions

Human motions are ubiquitous, and the active and efficient conversion of human motions to other forms of energy, such as light, offers a new possibility of energy-saving. Generally, ML materials are blended with polymer matrix (PDMS, Ecoflex, epoxy resin, etc.) and cast into films, however, the limited flexibility and compressibility of the films constraint the device performance and impede their application in the conversion of human motions to light energy. To address this issue, a porous sponge was constructed with the flexible, compressible, and self-luminous feature. The sponge was fabricated via the blade-coating method, with the sugar particles as the sacrificial template to create the porous structure (Figure 3A). The sugar was selected due to its low cost, ease of

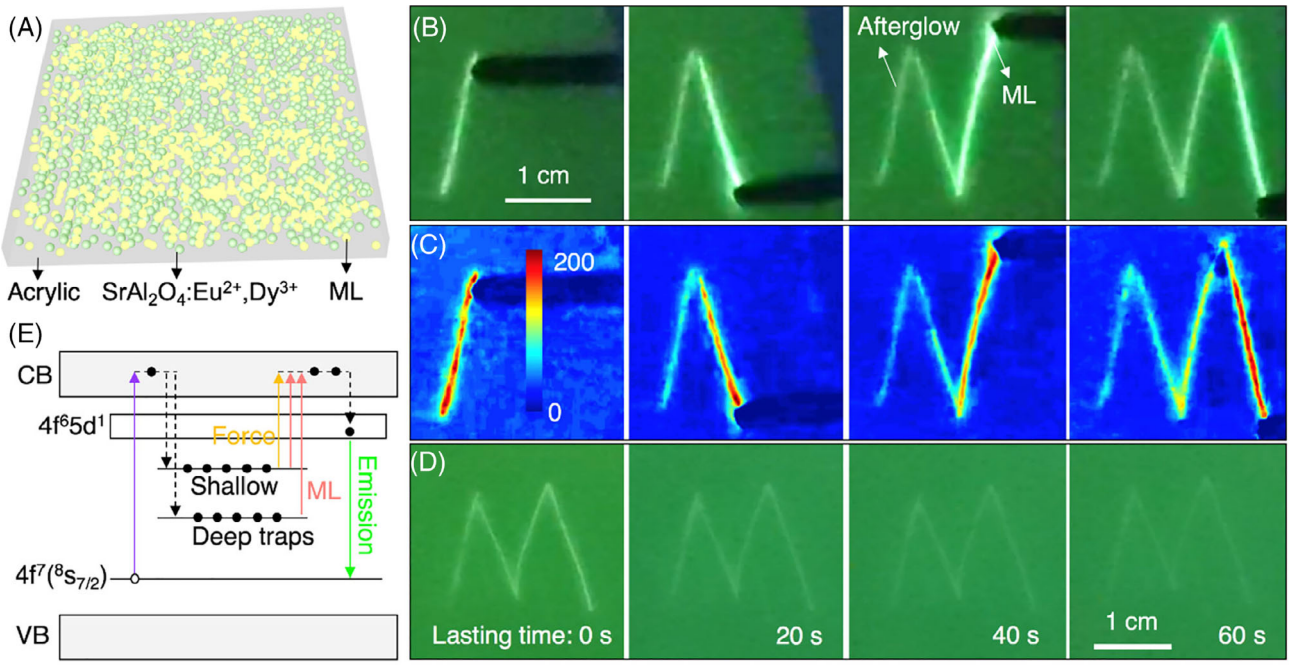

FIGURE 2 Visual sen-memory of the pressure. (A) Schematic of the device in conjunction of ML hybrids and phosphor embedded in acrylic matrix for the visual sen-memory of the pressure. (B,C) The photographs and the corresponding intensity maps of the device during the sen-memory process of the applied force. (D) The afterglow images of the device after the removal of the applied force. (E) Schematic illustration of the sen-memory mechanism

processing, and simple adjustment of pore size and porosity. The sponge was highly flexible and compressive, stemming from the porous structure, and yielded the strong ML emission upon pressing with fingers (Figure 3B,C and Video S7). Moreover, the ML emission of the sponge was much more obvious in comparison with the nonporous ones, as shown in Video S8. The enhanced ML emission of the sponge is attributed to the strong interaction between PDMS and ML hybrids enabled by the porous pores,[51] and the additional friction between the adjacent PDMS domains with the different curvatures,[52] leading to the improved mechanosensitivity as well as the stronger triboluminescence. The ML performance of the sponge could be further optimized by adjusting the porosity, determined by the weight ratio of ML hybrids to sugar. Among the different samples, the sponge with an ML hybrid:sugar ratio of 1:1 showed the optimal ML intensity (Figure 3D,E). The initial increase of the ML intensity originates from the sufficient friction of PDMS domains with the increasing porosity, and the subsequent decrease of ML intensity is due to the decreasing amount of the ML hybrids. The sponge also exhibited good stability over 1000 compression cycles at a strain of 50% (Figure 3F).

An array of the self-luminous sponge enabled the visual localization and imaging of the strain distribution owing to its flexibility and compressibility (Figure S13). As shown in Figure 3G, the sponge array composed of 11×13 pixels was fabricated, endowing the parallel readout of the strain applied to the device by a transparent stamp with the pattern of "SZU". Most importantly, the self-luminous sponge could be easily to be integrated into the shoes for the wearable applications due to its merits of lightweight, compressibility, and processability, allowing the conversion of the human movement into light emission and simultaneously eliminating the requirement of batteries and electrical cables (Figure 3H and Video S9). The self-luminous shoes could give intense ML emission during each step of walking. This feature not only enables the night-vision surveillance of human activities such as running at night, but also facilitates the self-powered sensing and recognition of human gait without having to sacrifice the artistry and comfortability of the shoes.

2.4 | Light generators for blue energy harvesting

Ocean covers more than 70% of the earth's surface, and the water wave energy is abundantly available without any interruption, regardless the weather.[53] Thus, harvesting of this "blue energy" represents a promising solution to the growing energy crisis. Commercial harvesters of blue energy such as hydropower turbines are

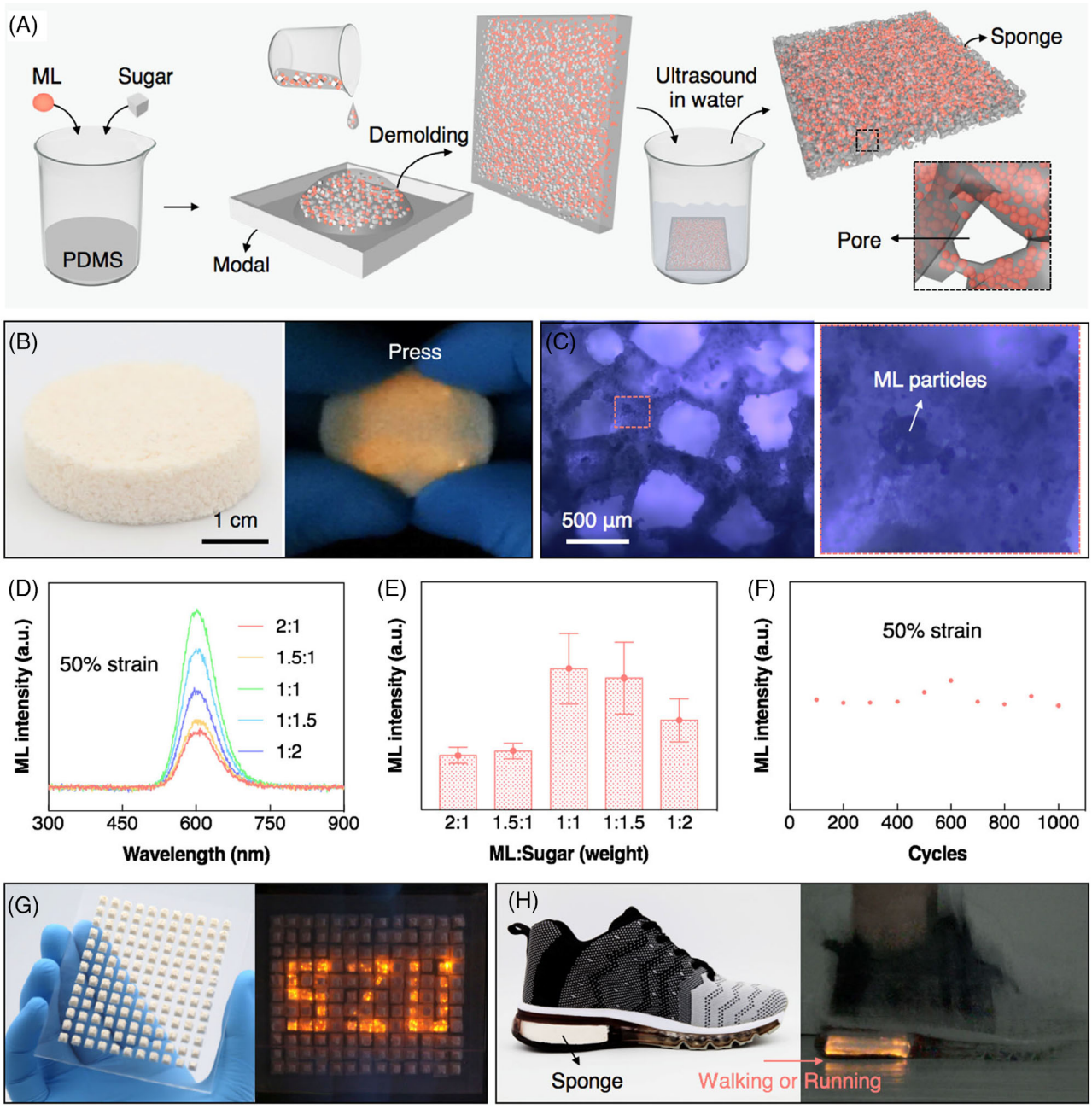

FIGURE 3 Self-luminous sponge. (A) The schematic fabrication of the flexible and compressible sponge with the self-luminous feature. (B) The photos of the self-luminous sponge, yielding the strong ML emission upon pressing by fingers. (C) The optical microscope images of the porous structure within the sponge. (D,E) The ML spectra and the integral ML intensities of the sponges with the different porosities determined by the ML material to sugar weight ratio at a strain of 50%. (F) The durability test of the self-luminous sponge over 1000 compression cycles at a strain of 50%. (G) A sponge array composed of 11 by 13 pixels for the visual localization and imaging of the strain distribution. (H) The self-luminous shoes for the conversion of human movement into light emission, enabling the self-powered night-vision surveillance of human activities such as running at night

based on the electromagnetic generators, which are large, heavy, expensive, and technically difficult to operate. The emerging triboelectric nanogenerators enabled by contact electrification and electrostatic induction represent a tangible alternative to the commercial harvesters, for example, the wave energy is harvested by the triboelectric mechanism and then converted to light emission by driving the light-emitting diodes.[54] However, triboelectric nanogenerators are still in their infancy, and the arrangement of electrical cables and the risk of electric leakage in water circumstance should also be considered.[39,55,56] Here, a novel light generator based on the ML mechanism is demonstrated, enabling the direct conversion

of blue energy into intense light emission without any electrical elements.

To fabricate the light generator, ML beads with a core–shell structure were first designed and produced via an in situ growth strategy (see Section 4 for details). The ML beads are composed of a ZrO_2 core surrounded by a shell layer of ML hybrid, as illustrated in Figure 4A, in which the shell layer is textured and densely grown on the ZrO_2 core, as indicated by their SEM images and EDS profiles (Figure 4B,C). The diameter of the ML hybrid@ZrO_2 core–shell beads could be easily tuned from 0.4 to 6 mm by adjusting the size of the ZrO_2 template, and all the prepared beads could generate intense ML upon shaking, as shown in Figure 4D. Furthermore, the ML hybrid@ZrO_2 core–shell beads exhibited exceptional mechanical stability. As shown in Figure 4E, the ML intensity of the beads, observed by naked eyes, did not attenuate noticeably after milling for 60 min at a speed of 450 r/min (27 000 cycles). The outstanding stability of the beads promises their long-term application in light generators.

The proposed light generator is schematically shown in Figure 5A, where the independent spherical light generators were connected to form a network that could float on the ocean surface. Such a spherical light generator is composed of a large number of the ML hybrid@ZrO_2 core–shell beads enclosed in a transparent acrylic container (Figure 5B), where the collisions among the ML hybrid@ZrO_2 core–shell beads dominate the ML emission. The light generator could emit the strong ML upon mechanical stimuli, and the emission color could be adjusted by changing the shell layer of ML hybrids (Figure 5C and Videos S10–S12). The significant brightness of the light generator can be

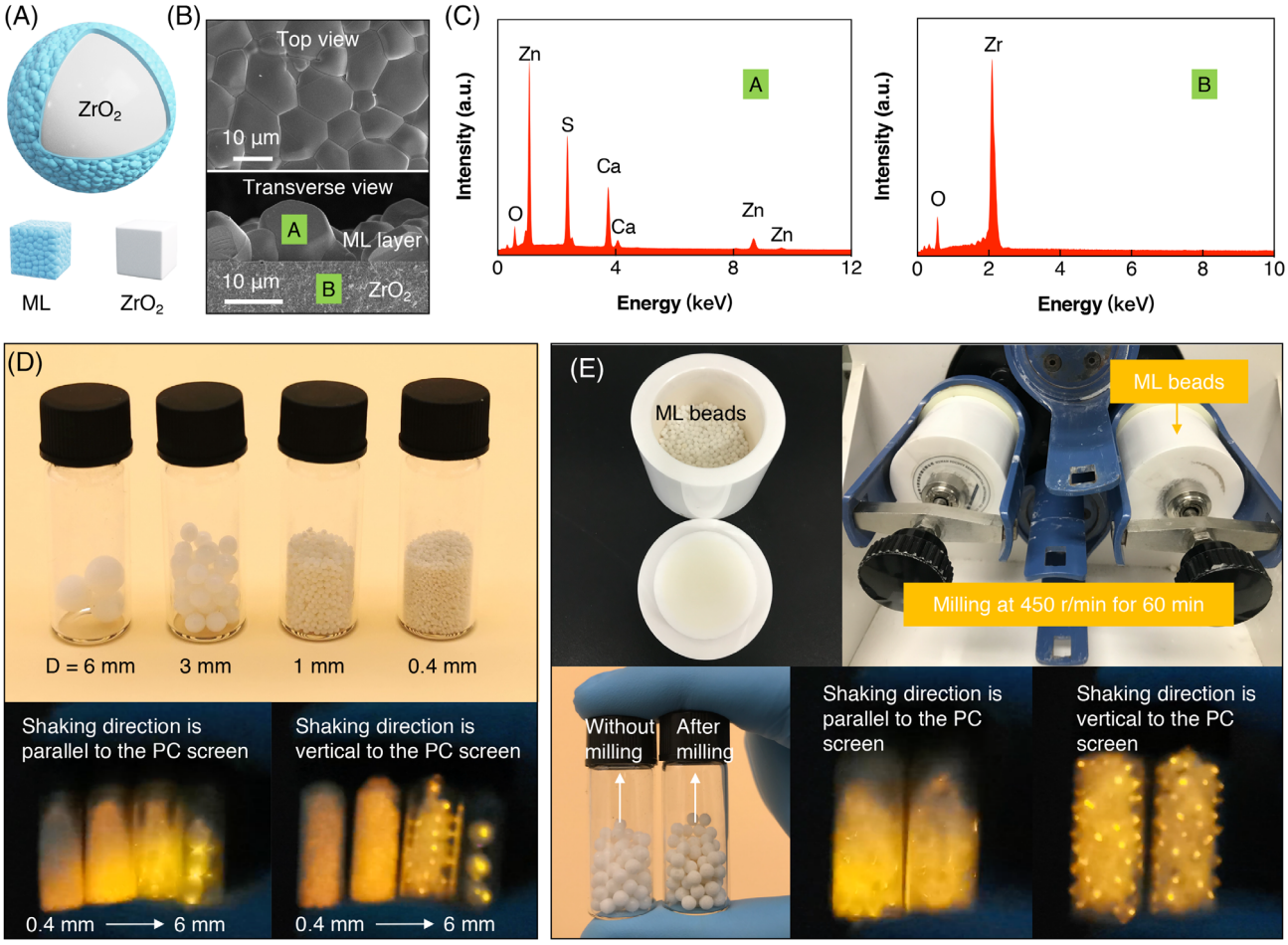

FIGURE 4 ML hybrid@ZrO_2 core–shell beads. (A) The schematic of the ML beads is composed of the ZrO_2 core and the shell layer of ML hybrid. (B,C) SEM images and EDS spectra of the ML hybrid@ZrO_2 core–shell beads, indicating the shell layer of the textured ML hybrid is tightly grown on the ZrO_2 core. (D) Optical images of the ML hybrid@ZrO_2 core–shell beads with the different diameters and their emission images upon shaking. (E) Photographs of the setup for the stability test of the ML hybrid@ZrO_2 core–shell beads, the ML intensity of the beads observed by naked eyes do not show any obvious attenuation after milling for 60 min at a speed of 450 r/min (27 000 cycles)

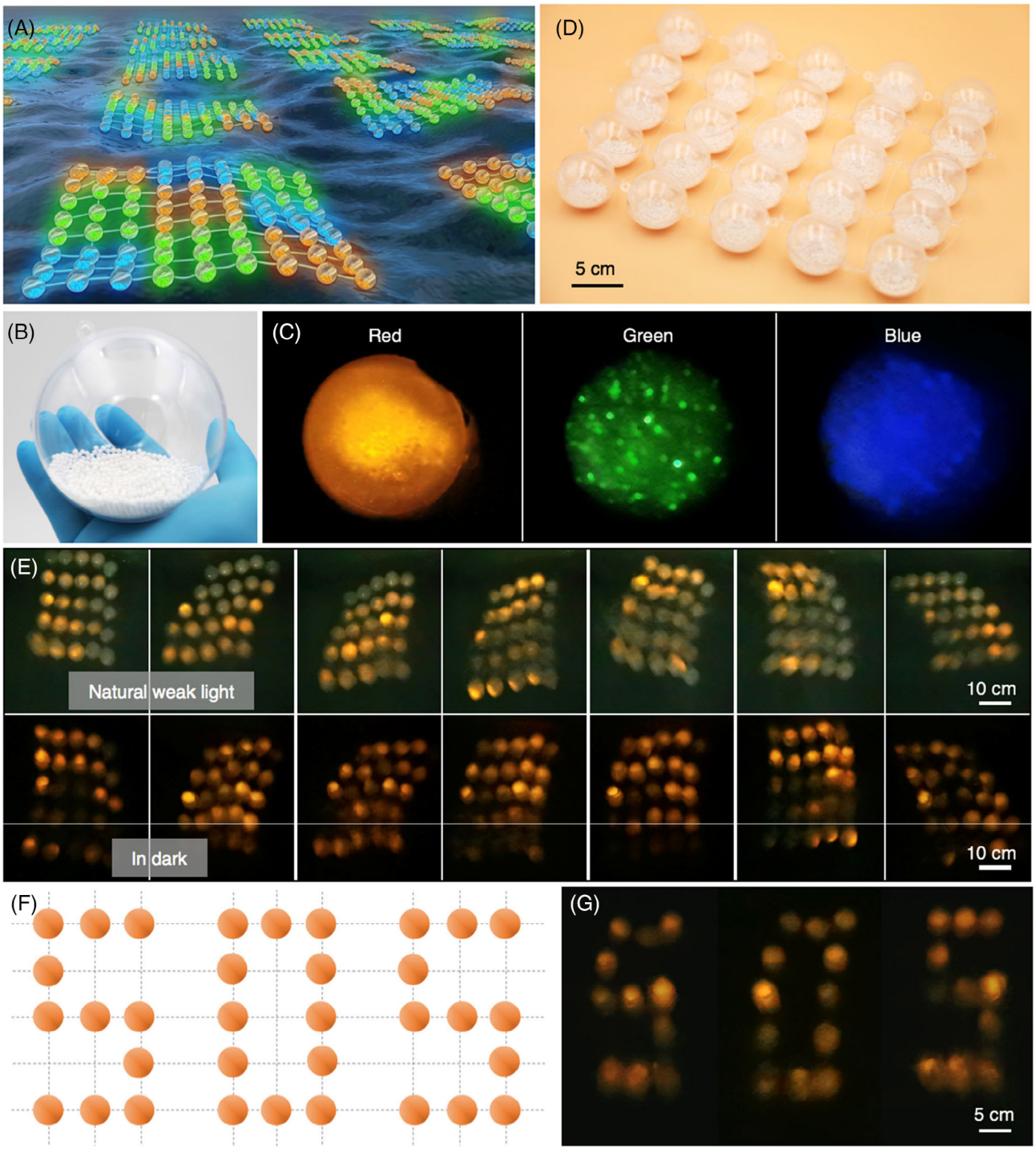

FIGURE 5 Light generators for blue energy harvesting. (A) Illustration of the light generators for the harvesting of blue energy. (B) The photograph of the independent spherical light generator, which is composed of a transparent acrylic shell and a heap of ML hybrid@ZrO_2 core–shell beads. (C) The spherical light generator can emit the strong ML upon shaking, and the emission color can be adjusted by changing the shell layer of ML hybrids. (D) Photograph of a representative light generator network consisting of 5 by 5 units. (E) The screenshot images of the light generator network driven by the water wave energy, exhibiting the dynamic formation and the bright light emission. (F) The schematic of the light generator network with the designed arrange. (G) The patterned display of the light generator network driven by water wave energy

attributed to the novel design of the ML hybrid@ZrO_2 beads with a core–shell structure, enabling the direct and efficient collision of the ML hybrids. This differs from the typical method of embedding the ML materials in a polymer matrix, which results in severe dissipation of the mechanical energy. Meanwhile, the ZrO_2 with a Young's

modulus of 545.12 GPa has the greatest stiffness, guaranteeing the concentration of stress onto ML hybrids.

Figure 5D shows the photograph of a representative light generator network consisting of 5 × 5 units, which is able to float on the water surface owing to the buoyant force. When driven by the water wave, the light generator network exhibits the dynamic formation and affords the bright light emission (Figure 5E and Video S13). Furthermore, a desired light-emitting pattern can be obtained with an appropriate distribution of the light generator in the network, enabling a customized display. Thus, significant applications can be realized in rescue, warning, and survival in wilderness (Figure 5F,G). In addition, the light generator is expected to be a ubiquitous light source, with a series of potential applications such as in water splitting, photocatalysis, and optical communication.

3 | CONCLUSIONS

In summary, we developed a simple method to convert the waste eggshells into high-performance ML hybrids. The ML hybrids can respond to a force as small as 5 N and exhibit an intense ML intensity that is two times higher than that of the commercial ZnS ML material. The ML hybrids are chemically stable, and the ML color can be regulated by changing the enriched activators. A self-powdered sen-memory panel was demonstrated by combining the ML hybrid with a phosphor, endowing the visual sensing and recording of the applied pressure over an extended duration of 1.5 min. A self-luminous sponge with the designed porous structure has been developed, enabling the self-luminous shoes for the conversion of human motions into light emission. Most importantly, a novel way of harvesting the blue energy using the developed light generator was also presented, holding great promise in emerging applications such as self-sustainable display, ubiquitous light source, water splitting, and photocatalysis. This work turns waste into treasure, inspiring the research dedication to waste recycling and utilization in burgeoning areas.

4 | MATERIALS AND METHODS

4.1 | Materials

The waste eggshells are collected from the local market. ZnS (99.99% metals basis, 3.3–4.3 μm, Aladdin), $MnCO_3$ (≥99.9% trace metals basis, Sigma Aldrich), $Pr(NO_3)_3{\cdot}6H_2O$ (99.99%, Sinopharm Group Co. Ltd.), $Gd(NO_3)_3{\cdot}6H_2O$ (99.99%, Sinopharm Group Co. Ltd.), LiF (≥99.99% trace metals basis, Sigma-Aldrich), $PbCl_2$ (99.999%, metals basis, Alfa Aesar).

4.2 | Preparation of the eggshell powder

The eggshell powders were prepared by modifying a precious reported method.[57] The eggshells were ultrasonically cleaned in water for several times and the inner membranes can be partly removed by hand during the cleaning process. The cleaned eggshells were transferred to the ball mill with water and then mechanically crushed for 6 h. The water and inner membranes were removed by a manual precipitation process, which left a slurry mixture. The slurry mixture was dried in oven at a temperature of 105°C for overnight, and then was sieved through the 54 μm strainer. The residual inner membranes were further removed by heating the powders to a temperature of 300°C for a period of 2 h, and the products were milled again and sieved through the 20 μm strainer.

4.3 | Synthesis of the ML hybrids

Using the Mn-doped ML hybrids as a modal. The eggshell powder in conjunction with the ZnS powder and the $MnCO_3$ powder were mixed with a certain ratio of molar, for example, the Ca:Zn:Mn = 1:2:1 refers to the molar ratio of the $CaCO_3$ to ZnS to $MnCO_3$, where the content of $CaCO_3$ in the eggshell powder is estimated to be 90% by weight. The mixture was ground in the agate mortar with the assistance of the absolute ethyl alcohol for a few times, followed by a desiccation at 80°C for 4 h in oven and at a calcination at 1100°C for 4–6 h in the furnace under 80 sccm argon. The products were obtained after the furnace was naturally cooled to the room temperature, and then ground into the fine powder for use. The similar process was applied to the Pr- or Pb-doped ML hybrids, especially, the LiF and the $Gd(NO_3)_3{\cdot}6H_2O$ were used to promote the doping and improve the ML performance of the Pr-doped ML hybrids.

4.4 | Characterizations of the ML hybrids

The morphology and composition of the ML hybrids were characterized by a field-emission scanning electron microscope (SEM, FEI Nova NanoSEM 450) equipped with an EDAX. The XRD patterns were acquired using an x-ray diffractometer (PANalytical X'Pert 3 Powder) with a Cu Kα radiation source. The fluorescence microscope images were obtained by a Nikon Eclipse Ti-U inverted microscope equipped with a Nikon Digital Sight DS-Fi2 camera. The photoluminescence (PL) spectra and transient decay curves were obtained using an Edinburgh FLS1000 spectrometer. The x-ray photoelectron spectrum was recorded on the AULVAC-PHI Phi5000 VersaProbe III

XPS (Chigasaki, Japan, ULVAC-PHI). The ML performances were characterized by a home-made measurement apparatus consisting of the linear motor, dynamometer, and fiber optic spectrometer, where the samples were the ML hybrids sealed between two squared polyethylene glycol terephthalate sheets (3.5 cm × 3.5 cm).

4.5 | Fabrication and characterizations of the visual sen-memory panel

For the device of visual sensing of the pressure distribution, the ML hybrids are manually mixed with the acrylic part A at a weight ratio of 3:1 (ML to part A) for 5 min, and then the acrylic part B is added to the mixture with a weight ratio to ML of 2:3, and then continue to mix for 5 min. The mixture is transferred to the silicone mold and cure at room temperature for overnight. For the device of visual sen-memory of the pressure distribution, the ML hybrids, phosphor, and acrylic part A are mixed for 5 min at a weight ratio of 3:3:2, and then the acrylic part B is added to the mixture with a weight ratio to ML of 2:3, and then continue to mix for 5 min. The mixture is transferred to the silicone mold and cure at room temperature for overnight. The ML emission photos are taken by a camera (Canon EOS 5D, f 4.5, expose time is 5 s), and the ML videos are taken by a mobile phone (HUAWEI P30).

4.6 | Fabrication and characterizations of the ML sponge

The sponge is fabricated via the blade coating method with the sugar particles as the sacrificing template to make the porous structure, as illustrated in Figure 4A. In detail, the ML hybrids, sugar particles with the grain size of 300–500 μm and the PDMS matrix with a designed weight ratio are poured into the plastic beaker and uniformly mixed. The mixture is transfer the acrylic mold with a certain thickness and then pressed into the tightly stacked film, and the redundant mixture is removed using the blade. The film is cured at 60°C for 24 h in the oven, and then is demolded and put in the beaker with water for the ultrasonic bath to completely dissolve the sugar particles. The size, shape, and thickness of the sponge can be adjusted by designing the mold, and the porosity of the sponge can be adjusted by changing the weight ratio of the ML hybrids to sugar particles. The ML performances were characterized by a home-made measurement apparatus consisting of the linear motor, dynamometer, and fiber optic spectrometer. The ML emission photos are taken by a camera (Canon EOS 5D, f 4.5, expose time is 2 s), and the ML videos are taken by a mobile phone (HUAWEI P30).

4.7 | Preparation and applications of the ML hybrid@ZrO_2 core–shell beads

The ML hybrid@ZrO_2 core–shell beads are prepared by the high temperature solid state reaction similar to the synthesis of the ML hybrids. The ZrO_2 beads are ultrasonically clean with acetone, isopropanol, deionized water, and dry at 100°C for 1 h in the oven. The cleaned ZrO_2 beads are dropped into the grounded raw materials that are used to prepare the ML hybrids, and go through the program as same as the high temperature synthesis of the ML hybrids. The products are milled for certain times and then sieved out the ML powder to obtain the ML hybrid@ZrO_2 core–shell beads. The ML hybrid@ZrO_2 core–shell beads are transferred to the transparent acrylic ball, and then seal the acrylic ball by the acrylic precursor to obtain the spherical light generator. The light generator network is formed by connecting the independent spherical light generator using fish wires. The water wave is generated by a commercial water pump. The ML videos are taken by a mobile phone (HUAWEI P30).

ACKNOWLEDGMENTS

The authors thank Professor Feng Wang at City University of Hong Kong and Professor Bolong Huang at The Hong Kong Polytechnic University for their valuable and constructive discussion on this manuscript. This work was supported by the National Natural Science Foundation of China (No. U20A20166, 61675027, 51622205, 51432005, 61805015, 61804011, 61505010, 61875136, 52125205, and 52002246), Fundamental Research Project of Guangdong Province (2020A1515011315), Beijing City Committee of Science and Technology (Z171100002017019, Z181100004418004), Beijing Natural Science Foundation (Z180011), Natural Science Foundation of Beijing Municipality (Z180011), Shenzhen Fundamental Research Project (JCYJ20190808170601664 and 201708183000260), Science and Technology Innovation Project of Shenzhen Excellent Talents (RCBS20200714114919006).

CONFLICT OF INTEREST

The authors declare no conflict of interest.

ORCID

Caofeng Pan https://orcid.org/0000-0001-6327-9692

REFERENCES

1. Ma Y, Yu Y, Li J, et al. Stimuli-responsive photofunctional materials for green and security printing. *InfoMat*. 2021;3(1):82-100.
2. Yang J, Fang M, Li Z. Stimulus-responsive room temperature phosphorescence in purely organic luminogens. *InfoMat*. 2020;2(5):791-806.

3. Wang X, Zhang H, Yu R, et al. Dynamic pressure mapping of personalized handwriting by a flexible sensor matrix based on the mechanoluminescence process. *Adv Mater*. 2015;27(14):2324-2331.
4. Jang J, Kim H, Ji S, et al. Mechanoluminescent, air-dielectric MoS_2 transistors as active-matrix pressure sensors for wide detection ranges from footsteps to cellular motions. *Nano Lett*. 2020;20(1):66-74.
5. Wang C, Yu Y, Yuan Y, et al. Heartbeat-sensing mechanoluminescent device based on a quantitative relationship between pressure and emissive intensity. *Matter*. 2020;2(1):181-193.
6. Zhang H, Peng D, Wang W, et al. Mechanically induced light emission and infrared-laser-induced upconversion in the Er-doped CaZnOS multifunctional piezoelectric semiconductor for optical pressure and temperature sensing. *J Phys Chem C*. 2015;119(50):28136-28142.
7. Zhao XJ, Kuang SY, Wang ZL, et al. Electricity-free electroluminescence excited by droplet impact driven triboelectric field on solid−liquid interface. *Nano Energy*. 2020;75:104823.
8. Li L, Wondraczek L, Peng M, et al. Force-induced 1540 nm luminescence: role of piezotronic effect in energy transfer process for mechanoluminescence. *Nano Energy*. 2020;69:104413.
9. Song S, Song B, Cho C-H, et al. Textile-fiber-embedded multiluminescent devices: a new approach to soft display systems. *Mater Today*. 2020;32:46-58.
10. Jeong SM, Song S, Kim H, et al. Mechanoluminescence color conversion by spontaneous fluorescent-dye-diffusion in elastomeric zinc sulfide composite. *Adv Funct Mater*. 2016;26(27):4848-4858.
11. Shi X, Zuo Y, Zhai P, et al. Large-area display textiles integrated with functional systems. *Nature*. 2021;591(7849):240-245.
12. Jeong SM, Song S, Kim H. Simultaneous dual-channel blue/green emission from electro-mechanically powered elastomeric zinc sulphide composite. *Nano Energy*. 2016;21:154-161.
13. Liu L, Xu C-N, Yoshida A, et al. Scalable elasticoluminescent strain sensor for precise dynamic stress imaging and onsite infrastructure diagnosis. *Adv Mater Tech*. 2019;4(1):1800336.
14. Wang X, Peng D, Huang B, et al. Piezophotonic effect based on mechanoluminescent materials for advanced flexible optoelectronic applications. *Nano Energy*. 2019;55:389-400.
15. Chen C, Zhuang Y, Tu D, et al. Creating visible-to-near-infrared mechanoluminescence in mixed-anion compounds $SrZn_2S_2O$ and SrZnSO. *Nano Energy*. 2020;68:104329.
16. Tu D, Xu C-N, Yoshida A, et al. $LiNbO_3:Pr^{3+}$: a multipiezo material with simultaneous piezoelectricity and sensitive piezoluminescence. *Adv Mater*. 2017;29(22):1606914.
17. Jiang T, Zhu Y-F, Zhang J-C, et al. Multistimuli-responsive display materials to encrypt differentiated information in bright and dark fields. *Adv Funct Mater*. 2019;0(0):1906068.
18. Zhang J-C, Pan C, Zhu Y-F, et al. Achieving thermo-mechano-opto-responsive bitemporal colorful luminescence via multiplexing of dual lanthanides in piezoelectric particles and its multidimensional anticounterfeiting. *Adv Mater*. 2018;30(49):1804644.
19. Kamimura S, Xu C-N, Yamada H, et al. Near-infrared luminescence from double-perovskite $Sr_3Sn_2O_7:Nd^{3+}$: a new class of probe for in vivo imaging in the second optical window of biological tissue. *J Cerma Soc Jpn*. 2017;125(7):591-595.
20. Xiong P, Peng M, Cao J, et al. Near infrared mechanoluminescence from $Sr_3Sn_2O_7$: Nd^{3+} for in situ biomechanical sensor and dynamic pressure mapping. *J Am Ceram Soc*. 2019;102(10):5899-5909.
21. Tu D, Xu C-N, Kamimura S, et al. Ferroelectric $Sr_3Sn_2O_7:Nd^{3+}$: a new multipiezo material with ultrasensitive and sustainable near-infrared piezoluminescence. *Adv Mater*. 2020;32(25):1908083.
22. Jeong SM, Song S, Joo K-I, et al. Bright, wind-driven white mechanoluminescence from zinc sulphide microparticles embedded in a polydimethylsiloxane elastomer. *Energ Environ Sci*. 2014;7(10):3338-3346.
23. Chen Y, Zhang Y, Karnaushenko D, et al. Addressable and color-tunable piezophotonic light-emitting stripes. *Adv Mater*. 2017;29(19):1605165.
24. Wong M-C, Chen L, Bai G, et al. Temporal and remote tuning of piezophotonic-effect-induced luminescence and color gamut via modulating magnetic field. *Adv Mater*. 2017;29(43):1701945.
25. Qian X, Cai Z, Su M, et al. Printable skin-driven mechanoluminescence devices via nanodoped matrix modification. *Adv Mater*. 2018;30(25):1800291.
26. Wu X, Zhu X, Chong P, et al. Sono-optogenetics facilitated by a circulation-delivered rechargeable light source for minimally invasive optogenetics. *Proc Natl Acad Sci*. 2019;116(52):26332-26342.
27. Hong G. Seeing the sound. *Science*. 2020;369(6504):638-638.
28. Du Y, Jiang Y, Sun T, et al. Mechanically excited multicolor luminescence in lanthanide ions. *Adv Mater*. 2019;31(7):1807062.
29. Peng D, Jiang Y, Huang B, et al. A ZnS/CaZnOS heterojunction for efficient mechanical-to-optical energy conversion by conduction band offset. *Adv Mater*. 2020;32(16):1907747.
30. Mignardi S, Archilletti L, Medeghini L, et al. Valorization of eggshell biowaste for sustainable environmental remediation. *Sci Rep-UK*. 2020;10(1):2436.
31. Matsui H, Xu C-N, Liu Y, et al. Origin of mechanoluminescence from Mn-activated $ZnAl_2O_4$: triboelectricity-induced electroluminescence. *Phys Rev B*. 2004;69(23):235109.
32. Moon Jeong S, Song S, Lee S-K, et al. Mechanically driven light-generator with high durability. *Appl Phys Lett*. 2013;102(5):051110.
33. Mukhina MV, Tresback J, Ondry JC, et al. Single-particle studies reveal a nanoscale mechanism for elastic, bright, and repeatable ZnS:Mn mechanoluminescence in a low-pressure regime. *ACS Nano*. 2021;15(3):4115-4133.
34. Ma R, Wei X, Wang C, et al. Reproducible mechanical-to-optical energy conversion in Mn (II) doped sphalerite ZnS. *J Lumin*. 2021;232:117838.
35. Zhang L, Shi K, Wang Y, et al. Unraveling the anomalous mechanoluminescence intensity change and pressure-induced red-shift for manganese-doped zinc sulfide. *Nano Energy*. 2021;85:106005.
36. Chandra VK, Chandra BP, Jha P. Strong luminescence induced by elastic deformation of piezoelectric crystals. *Appl Phys Lett*. 2013;102(24):241105.
37. Sage I, Bourhill G. Triboluminescent materials for structural damage monitoring. *J Mater Chem*. 2001;11(2):231-245.
38. Zhang J-C, Wang X, Marriott G, et al. Trap-controlled mechanoluminescent materials. *Prog Mater Sci*. 2019;103:678-742.
39. Zhou K, Zhao Y, Sun X, et al. Ultra-stretchable triboelectric nanogenerator as high-sensitive and self-powered electronic skins for energy harvesting and tactile sensing. *Nano Energy*. 2020;70:104546.
40. Peng X, Dong K, Ye C, et al. A breathable, biodegradable, antibacterial, and self-powered electronic skin based on all-nanofiber triboelectric nanogenerators. *Sci Adv*. 2020;6(26):eaba9624.

41. Wang X, Qiu Z, Li Y, et al. Core–shell structured CaS:Eu^{2+}@CaZnOS via inward erosion growth to realize a super stable chalcogenide red phosphor. *J Mater Chem C*. 2019;7(20):5931-5936.
42. Zhang G, Wang X. Oxysulfide semiconductors for photocatalytic overall water splitting with visible light. *Angew Chem Int Ed*. 2019;58(44):15580-15582.
43. Chen Y, Lei Y, Li Y, et al. Strain engineering and epitaxial stabilization of halide perovskites. *Nature*. 2020;577(7789):209-215.
44. Wang C, Dong L, Peng D, et al. Tactile sensors for advanced intelligent systems. *Adv Intell Syst*. 2019;1(8):1900090.
45. Peng Y, Lu J, Peng D, et al. Dynamically modulated GaN whispering gallery lasing mode for strain sensor. *Adv Funct Mater*. 2019;29(42):1905051.
46. Wang C, Pan C, Wang Z. Electronic skin for closed-loop systems. *ACS Nano*. 2019;13(11):12287-12293.
47. Liu H, Li Q, Bu Y, et al. Stretchable conductive nonwoven fabrics with self-cleaning capability for tunable wearable strain sensor. *Nano Energy*. 2019;66:104143.
48. Ren J, Zhang W, Wang Y, et al. A graphene rheostat for highly durable and stretchable strain sensor. *InfoMat*. 2019;1(3):396-406.
49. Petit RR, Michels SE, Feng A, et al. Adding memory to pressure-sensitive phosphors. *Light Sci Appl*. 2019;8(1):124.
50. Zhuang Y, Tu D, Chen C, et al. Force-induced charge carrier storage: a new route for stress recording. *Light Sci Appl*. 2020;9(1):182.
51. Park J, Lee Y, Barbee MH, et al. A hierarchical nanoparticle-in-micropore architecture for enhanced mechanosensitivity and stretchability in mechanochromic electronic skins. *Adv Mater*. 2019;31(25):1808148.
52. Xu C, Zhang B, Wang AC, et al. Contact-electrification between two identical materials: curvature effect. *ACS Nano*. 2019;13(2):2034-2041.
53. Leung S-F, Fu H-C, Zhang M, et al. Blue energy fuels: converting ocean wave energy to carbon-based liquid fuels via CO_2 reduction. *Energ Environ Sci*. 2020;13(5):1300-1308.
54. Wu H, Wang Z, Zi Y. Multi-mode water-tube-based triboelectric nanogenerator designed for low-frequency energy harvesting with ultrahigh volumetric charge density. *Adv Energy Mater*. 2021;11(16):2100038.
55. Rodrigues C, Nunes D, Clemente D, et al. Emerging triboelectric nanogenerators for ocean wave energy harvesting: state of the art and future perspectives. *Energ Environ Sci*. 2020;13(9):2657-2683.
56. Jiang D, Ouyang H, Shi B, et al. A wearable noncontact free-rotating hybrid nanogenerator for self-powered electronics. *InfoMat*. 2020;2(6):1191-1200.
57. Cree D, Rutter A. Sustainable bio-inspired limestone eggshell powder for potential industrialized applications. *ACS Sustain Chem Eng*. 2015;3(5):941-949.

SUPPORTING INFORMATION

Additional supporting information may be found in the online version of the article at the publisher's website. [Correction added on 30 September 2021, after first online publication: Supporting information has been updated online].

How to cite this article: Wang C, Ma R, Peng D, et al. Mechanoluminescent hybrids from a natural resource for energy-related applications. *InfoMat*. 2021;3(11):1272-1284. doi:10.1002/inf2.12250